Vol 464|18 March 2010|doi:10.1038/nature08840

LETTERS

Isotope fractionation in silicate melts by thermal diffusion

F. Huang[1]†*, P. Chakraborty[1]*, C. C. Lundstrom[1], C. Holmden[2], J. J. G. Glessner[1], S. W. Kieffer[1] & C. E. Lesher[3]

The phenomenon of thermal diffusion (mass diffusion driven by a temperature gradient, known as the Ludwig–Soret effect[1,2]) has been investigated for over 150 years, but an understanding of its underlying physical basis remains elusive. A significant hurdle in studying thermal diffusion has been the difficulty of characterizing it. Extensive experiments over the past century have established that the Soret coefficient, S_T (a single parameter that describes the steady-state result of thermal diffusion), is highly sensitive to many factors[3–9]. This sensitivity makes it very difficult to obtain a robust characterization of thermal diffusion, even for a single material. Here we show that for thermal diffusion experiments that span a wide range in composition and temperature, the difference in S_T between isotopes of diffusing elements that are network modifiers (iron, calcium and magnesium) is independent of the composition and temperature. On the basis of this finding, we propose an additive decomposition for the functional form of S_T and argue that a theoretical approach based on local thermodynamic equilibrium[3,5,10] holds promise for describing thermal diffusion in silicate melts and other complex solutions. Our results lead to a simple and robust framework for characterizing isotope fractionation by thermal diffusion in natural and synthetic systems.

In 1856, Carl Ludwig discovered an intriguing phenomenon[1] (that was tested in 1879 by Charles Soret[2]): when a homogeneous salt solution in a column is subjected to a temperature gradient, the salt preferentially diffuses against the temperature gradient, from the hot end to the cold end. This phenomenon—mass diffusion driven by a temperature gradient—is called thermal diffusion or the Ludwig–Soret effect[2]. Thermal diffusion has been suggested to have a role in a number of phenomena, including the origin of life, via migration and concentration of DNA along temperature gradients[11]; the seasonal temperature-driven fractionation of nitrogen and argon isotopes in the air trapped in polar ice[12,13]; and the differentiation of igneous rocks[14]. Furthermore, thermal diffusion shows great potential in emerging technological applications[5,8,11] from nanotechnology to biotechnology. Despite the long history and wide importance of this phenomenon, the physics of thermal diffusion remains poorly understood[3,7–10].

Consider a dilute, homogeneous concentration of guest particles suspended in a host liquid (a simple binary mixture), for example salt in water. When a temperature gradient, ∇T, is applied across the mixture, thermal diffusion causes the particles to migrate (usually from the hot to the cold end) with a mass flux $-D_T C\nabla T$, where D_T is the thermal diffusion coefficient and C is the concentration. The migration of the particles sets up a concentration gradient, which in turn causes chemical diffusion of particles with a mass flux $D\nabla C$, where D is the chemical diffusion coefficient, in the opposite direction to thermal diffusion. In the steady state, these two fluxes balance each other, thereby leading to[9,15]

$$\mathrm{d}C/C = -S_T\,\mathrm{d}T \quad (1)$$

where S_T, the Soret coefficient, equals D_T/D and is the single parameter that determines the magnitude of the resultant concentration gradient in the steady state. Extensive experimental data over the last century show that S_T is markedly sensitive to conditions. For instance, the magnitude and sign of S_T can change drastically as a function of a variety of parameters[4,6,8–10] including, but not limited to, the chemical composition of the system, the size and charge of the particle, and the temperature. In many cases, the functional form of S_T is unknown. The sensitive and unknown functional dependence of S_T poses a significant practical problem: similar systems may be characterized by different values of S_T, requiring that the value of S_T be individually determined for each system.

Our focus is on isotope fractionation through thermal diffusion in silicate melts. We limit our attention to the steady state of thermal diffusion and, furthermore, to the isotopic fractionation of iron, calcium and magnesium (which break up the polymerization of the silicate melt and are thus termed network modifiers), and do not consider network formers (for example silicon and oxygen, which form tetrahedron networks in silicate melts). Although multicomponent silicate melts are different from the simple binary mixtures discussed above, they are analysed as a pseudo-binary system[6,16–18] in the framework of equation (1). In this system, the silicate melt is the host liquid, albeit with a complex structure, and the isotopes are the guest particles in the melt. Similar to previous studies of thermal diffusion in other systems[3,4,8,9,19,20], thermal diffusion experiments on silicate melts show the marked sensitivity of S_T to the details of the system. For instance, in the case of thermal diffusion of potassium, changing the bulk composition of the melt from basalt to rhyolite changes the value of S_T from -5.5×10^{-3} to $0.89\times10^{-3}\,^{\circ}\mathrm{C}^{-1}$ (refs 6, 16). Furthermore, there exists no theoretical framework for obtaining a functional form of S_T for thermal diffusion in silicate melts[17,18,21–23]. Instead, such systems are characterized using empirical formulae; see, for example, refs 6, 16–18. Here we seek to use the properties of isotopes, namely their almost identical chemical properties but distinctly different masses, to bypass the complexities of chemical interactions and characterize isotopic fractionation through thermal diffusion in a simple framework. Ultimately, our objective is to propose a robust method for characterizing isotopic thermal diffusion in silicate melts and gain insight into the functional dependence of S_T.

We measured iron, magnesium and calcium isotope ratios of microdrilled samples from different positions (and hence at different temperatures) in elongate capsules of quenched silicate melt produced in

[1]Department of Geology, University of Illinois, Urbana, Illinois 61801, USA. [2]Department of Geological Sciences, University of Saskatchewan, Saskatoon, Saskatchewan S7N 5E2, Canada. [3]Department of Geology, University of California, Davis, California 95616, USA. †Present address: Institute of Geochemistry and Petrology, ETH Zurich, CH-8092 Zurich, Switzerland.
*These authors contributed equally to this work.

Table 1 | Iron, calcium and magnesium isotope data from thermal diffusion samples

		$\delta^{56}Fe_{IRMM-014}$ (‰)	2σ (‰)	$\delta^{57}Fe_{IRMM-014}$ (‰)	2σ (‰)	N	$\delta^{25}Mg_{DSM-3}$ (‰)	2σ (‰)	$\delta^{26}Mg_{DSM-3}$ (‰)	2σ (‰)	N	$\delta^{44}Ca_{SW}$ (‰)	2σ (‰)	N	T (°C)
ZM70, 46 h,	ZM70A	−2.45	0.22	−3.70	0.77	2	−3.40	0.02	−6.59	0.13	3	—	—	—	1,518
Mt Hood andesite,	ZM70B	−0.18	0.04	−0.24	0.15	2	−1.39	0.04	−2.70	0.03	3	—	—	—	1,485
$\Delta T_{A-C} = 164$ °C, $T_0 = 1{,}430$ °C,	ZM70C	1.65	0.07	2.45	0.30	2	1.76	0.06	3.46	0.13	3	—	—	—	1,354
$\Omega_{Fe} = 0.0125$‰ °C^{-1} AMU^{-1},	Starting	0.06	0.05	0.09	0.05	4	−0.20	0.05	−0.40	0.09	4	—	—	—	—
$\Omega_{Mg} = 0.0307$‰ °C^{-1} AMU^{-1}	material														
ZM71, 168 h,	ZM71A	−3.00	0.09	−4.38	0.15	5	−5.15	0.07	−9.98	0.08	4	—	—	—	1,550
Mt Hood andesite,	ZM71B	−1.52	0.05	−2.22	0.14	5	−2.01	0.15	−3.90	0.09	4	—	—	—	1,503
$\Delta T_{A-D} = 270$ °C, $T_0 = 1{,}445$ °C,	ZM71C	1.07	0.06	1.60	0.12	4	0.96	0.07	1.82	0.08	5	—	—	—	1,402
$\Omega_{Fe} = 0.0113$‰ °C^{-1} AMU^{-1},	ZM71D	3.10	0.06	4.64	0.15	4	3.42	0.17	6.74	0.32	4	—	—	—	1,280
$\Omega_{Mg} = 0.0309$‰ °C^{-1} AMU^{-1}															
ZM98, 264 h,	ZM98A	−2.84	0.18	−4.21	0.29	3	−5.46	0.04	−10.70	0.04	4	−8.26	0.06	1	1,648
mid-ocean-ridge basalt,	ZM98B	−0.38	0.10	−0.60	0.21	3	−1.15	0.08	−2.28	0.10	4	−1.73	0.04	1	1,560
$\Delta T_{A-C} = 274$ °C, $T_0 = 1{,}531$ °C,	ZM98C	4.91	0.05	7.29	0.14	3	5.49	0.04	10.74	0.08	4	8.38	0.03	1	1,374
$\Omega_{Fe} = 0.0142$‰ °C^{-1} AMU^{-1},	Starting	0.24	0.05	0.36	0.13	4	−0.15	0.09	−0.33	0.07	4	−0.95	0.03	1	—
$\Omega_{Mg} = 0.0387$‰ °C^{-1} AMU^{-1},	material														
$\Omega_{Ca} = 0.0152$‰ °C^{-1} AMU^{-1}															
ZM99, 207 h,	ZM99A	−1.82	0.05	−2.70	0.09	3	—	—	—	—	—	—	—	—	1,645
0.46:0.8:0.46 fayalite:leucite:quartz,	ZM99B	0.86	0.07	1.27	0.09	3	—	—	—	—	—	—	—	—	1,537
$\Delta T_{A-C} = 247$ °C, $T_0 = 1{,}553$ °C,	ZM99C	3.30	0.06	4.91	0.08	3	—	—	—	—	—	—	—	—	1,398
$\Omega_{Fe} = 0.0104$‰ °C^{-1} AMU^{-1}	Starting	0.33	0.06	0.48	0.10	4	—	—	—	—	—	—	—	—	—
	material														
ZM100, 166 h,	ZM100A	−2.25	0.28	−3.48	0.46	2	—	—	—	—	—	—	—	—	1,645
pantellerite,	ZM100B	−1.67	0.04	−2.51	0.18	2	—	—	—	—	—	—	—	—	1,566
$\Delta T_{A-C} = 194$ °C, $T_0 = 1{,}536$ °C,	ZM100C	3.24	0.21	4.82	0.48	4	—	—	—	—	—	—	—	—	1,451
$\Omega_{Fe} = 0.0141$‰ °C^{-1} AMU^{-1}	Starting	0.25	0.13	0.40	0.13	4	—	—	—	—	—	—	—	—	—
	material														

The δ values reported here are computed relative to a standard: IRMM-014 for iron, DSM-3 for magnesium and natural sea water (SW) for calcium. We note that δ relative to starting material equals δ relative to standard minus δ of starting material (relative to standard). Temperature is estimated assuming a parabolic temperature profile. T_0 is the temperature of the position in the thermal diffusion experiment where the isotope composition is identical to that of the starting material. To compute T_0 for any sample, we calculate the temperature for which the best-fit straight line in the plot of δ (relative to starting material) versus temperature difference (relative to the hot end) of each isotope pair passes through δ = 0 and average this temperature over the different isotope pairs in the sample. The respective ΔT values indicate the temperature differences between the micro-drilled positions. N, number of repeat measurements.

previously performed and characterized thermal diffusion experiments[6,16] (Methods). These experiments spanned a wide range of chemical compositions of starting materials and temperatures (Table 1).

To assess the timescale on which the steady-state distribution of isotopes is reached, we compared the results of two experiments with identical andesitic starting composition but different run durations: 46 h (ZM70) and 168 h (ZM71). Although the shorter run was only 60% evolved to the steady state in terms of its major-element composition[6,16], the two experiments did not differ significantly in terms of thermal-diffusion isotopic sensitivity, Ω (the magnitude of isotopic fractionation per temperature offset, expressed as parts per thousand per degree Celsius per atomic mass unit[12,18]; Fig. 1). Thus, the system reached the isotopic steady state within 46 h, meaning that isotope fractionation induced by thermal diffusion in these experiments is not a transient feature.

Typically, the data from thermal diffusion experiments are presented in plots of concentration versus temperature. We, however, start discussing our data in a context more typical of isotope fractionation experiments—plots of isotope ratio versus isotope ratio (Fig. 2). In this convention, the data are reported in δ notation:

$$\delta^X M = \left[\frac{(^X M/^Y M)_{\text{sample}}}{(^X M/^Y M)_{\text{starting material}}} - 1\right] \times 1{,}000‰ \qquad (2)$$

Here $^X M/^Y M$ is the ratio of isotopes $^X M$ and $^Y M$ (by convention, $X > Y$). This approach leads to a striking observation: despite significant differences in the compositions of the starting materials (from 45 to 70 wt% SiO_2), a wide span of average experimental temperatures and even the presence of coexisting mineral phases, the data, to first order, are linearly correlated (Fig. 2). This observation suggests that isotopic fractionation through thermal diffusion in silicate melts can be treated in a robust framework.

To proceed, we cast our experimental observations in a theoretical framework. First, we integrate equation (1) to determine the concentration distribution of an isotope $^X M$ from temperature T_0 (at the reference location) to temperature T (at the location of interest), obtaining

$$\frac{(^X M)_T}{(^X M)_{T_0}} = \exp\left[-\int_{T_0}^{T} (S_T)_{x_M}\, \mathrm{d}T\right] \qquad (3)$$

where S_T is an unknown function of X, the melt composition, the temperatures T_0 and T, and other parameters[6,8–11,24]. If S_T were a constant, the concentration of $^X M$ would be exponentially distributed

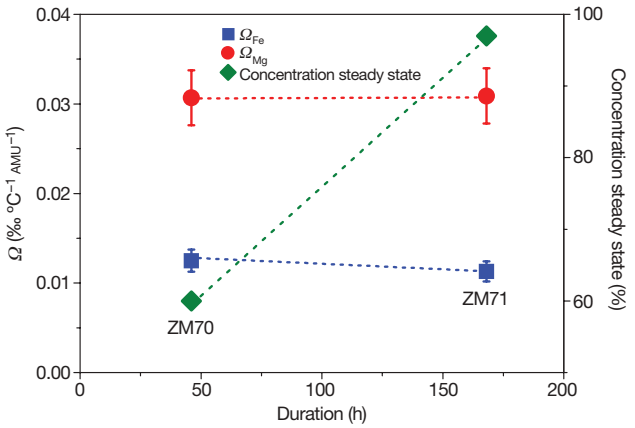

Figure 1 | Thermal-diffusion isotopic sensitivity and concentration steady state of time-series experiments (ZM70 and ZM71)[6]. The error bars (~10% relative error, 1σ) were calculated on the basis of errors in iron and magnesium isotope analyses and the temperature offset. The data labelled 'concentration steady state' corresponds to the fraction of the major-element concentration relative to its steady-state value[6]. We note that the approach to a steady-state isotopic distribution occurs faster than the compositional rearrangement of major elements in the silicate melt. This observation might be expected because isotopic diffusion is known to be faster than chemical diffusion and homogenization of isotope ratios occurs roughly according to the self-diffusivity of the element[26–29]. Assuming magnesium self-diffusivities of 7×10^{-11} m^2 s^{-1} in basaltic melt[25], the diffusion distance in 46 h is ~3.4 mm, which is similar to the length of the sample.

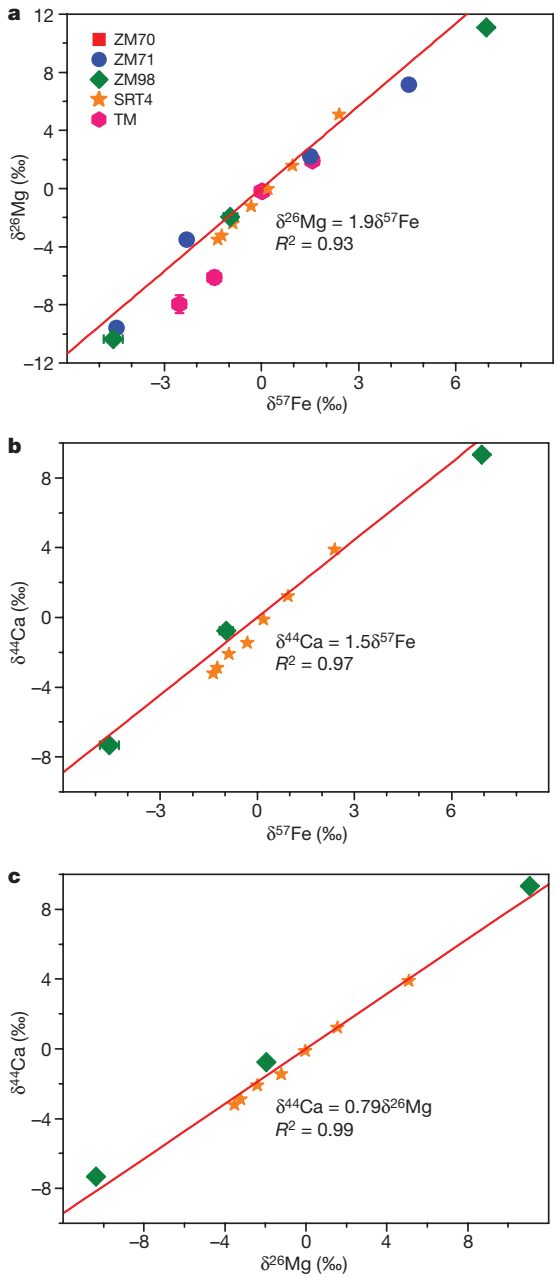

Figure 2 | Cross-correlations of magnesium, iron and calcium isotope ratios for both the thermal diffusion experiments of refs 6, 16 and previous work. The data form linear relationships for experiments spanning a wide range of melt compositions and temperatures, even in the presence of coexisting minerals. **a**, δ^{26}Mg versus δ^{57}Fe for ZM70, ZM71 and ZM98. Slopes defined by the previous studies (refs 6 and 17, 18 (thermal diffusion experiment, SRT4) and [30] (thermal migration experiment, TM)) are the same. **b**, **c**, δ^{44}Ca versus δ^{57}Fe (**b**) and δ^{44}Ca versus δ^{26}Mg (**c**) for ZM98 and SRT4. Symbols as in **a**. Most error bars (2σ; Table 1) are smaller than the symbols. R^2, coefficient of determination.

as a function of the temperature difference, $\Delta T = T - T_0$ (the plot of the concentration of ^XM versus ΔT on a log–linear scale would be linear). We, however, find that the concentrations of the isotopes (even for the same melt composition) are not distributed in this way (Fig. 3a–c). Instead, on the log–linear plot of the concentration of ^XM versus ΔT, the data from the different experiments are widely scattered (with the concentration in one sample changing by an order of magnitude) in the form of nonlinear, intersecting lines. Thus, the concentration distribution of isotopes in silicate melts cannot be characterized by a constant S_T.

We now consider the concentration distribution of the ratio of two isotopes, ^XM and ^YM. From equations (2) and (3), and using the fact that $\delta^XM \ll 1$, we obtain

$$\delta^X M \approx \ln\frac{(^XM/^YM)_T}{(^XM/^YM)_{T_0}} = \ln\frac{(^XM)_T}{(^XM)_{T_0}} - \ln\frac{(^YM)_T}{(^YM)_{T_0}} = -\int_{T_0}^{T}\Delta S_T\,dT \quad (4)$$

where $\Delta S_T = (S_T)_{^XM} - (S_T)_{^YM}$ (Supplementary Information). Notably, we find that in contrast to individual isotope concentrations (Fig. 3a–c), to first order each isotope ratio has a single exponential distribution as a function of ΔT for all experiments (or, equivalently, in δ notation the data for each isotope is, to first order, linearly distributed as a function of ΔT; Fig. 3d–f). This finding indicates that ΔS_T is independent of the melt composition and temperature. Thus, ΔS_T is a constant for pairs of isotopes of the same element. With a constant ΔS_T, equation (4) implies that δ^XM is linearly proportional to ΔT, which in turn manifests as the linear correlation in Fig. 2 (Supplementary Information). This constancy of ΔS_T for isotope ratios bears some similarity with its behaviour under thermal diffusion in simple binary liquid mixtures of benzene and cyclohexane: the difference in S_T of such mixtures with and without isotopic substitution is observed to be independent of concentration and temperature[19,20].

Given the composition and temperature independence of ΔS_T, we now turn to the problem of the functional form of S_T. We postulate the following additive decomposition of S_T:

$$S_T(m, \text{composition}, T, \ldots) = f_m(m, \ldots) + f_c(\text{composition}, T, \ldots) \quad (5)$$

Here m and T are atomic mass and temperature, respectively. The function f_m depends on m and other parameters (except melt composition and T), and the function f_c, which encapsulates the chemical effects, depends on melt composition, T and other parameters (except m). We now consider the significance of this equation for isotope fractionation through thermal diffusion. Because isotopes have nearly identical chemical properties and differ only in atomic mass (X and Y), two isotopes of an element have different values of f_m but the same value of f_c. Thus $\Delta S_T = f_m(X, \ldots) - f_m(Y, \ldots)$, wherein the chemical effects (f_c terms) have cancelled out. The functional form of equation (5) provides a strong constraint for a general theory of thermal diffusion in silicate melts—any theoretical prediction of the dependence of S_T on mass, composition and temperature can be decomposed according to equation (5). We note that the functional form of S_T for thermal diffusion in other systems[3,4,8,24] follows an additive decomposition similar to equation (5). Furthermore, the decomposition suggested in equation (5) provides guidance on seeking empirical formulae for S_T. For example, assuming that f_m depends on m and Z^2/a (the field strength, which correlates well with the self-diffusivity[25,26]; Z is the ionic charge and a is the ionic radius), our experimental data are best described by $f_m \propto m^{-1/4}(Z^2/a)^{9/20}$ (Supplementary Information).

Finally, we outline an approach for further theoretical work. Our examination of isotope ratios during thermal diffusion in silicate melts shows that they follow an exponential distribution that is characterized by a constant ΔS_T. Considerable theoretical progress has been made in understanding the thermal diffusion of particles in aqueous solutions[3,5,10], in which the concentration follows an equilibrium-like exponential distribution. This non-equilibrium process can be described in the framework of local thermodynamic equilibrium—a theoretical expression for S_T is obtained by relating the exponential distribution of concentration to the local Boltzmann law[3,5,10]. We submit that a similar approach, in which the variation of isotope ratio and the corresponding ΔS_T are analogous to the concentration of particles and the corresponding S_T, respectively, may yield further insights into the physics of thermal diffusion in silicate melts.

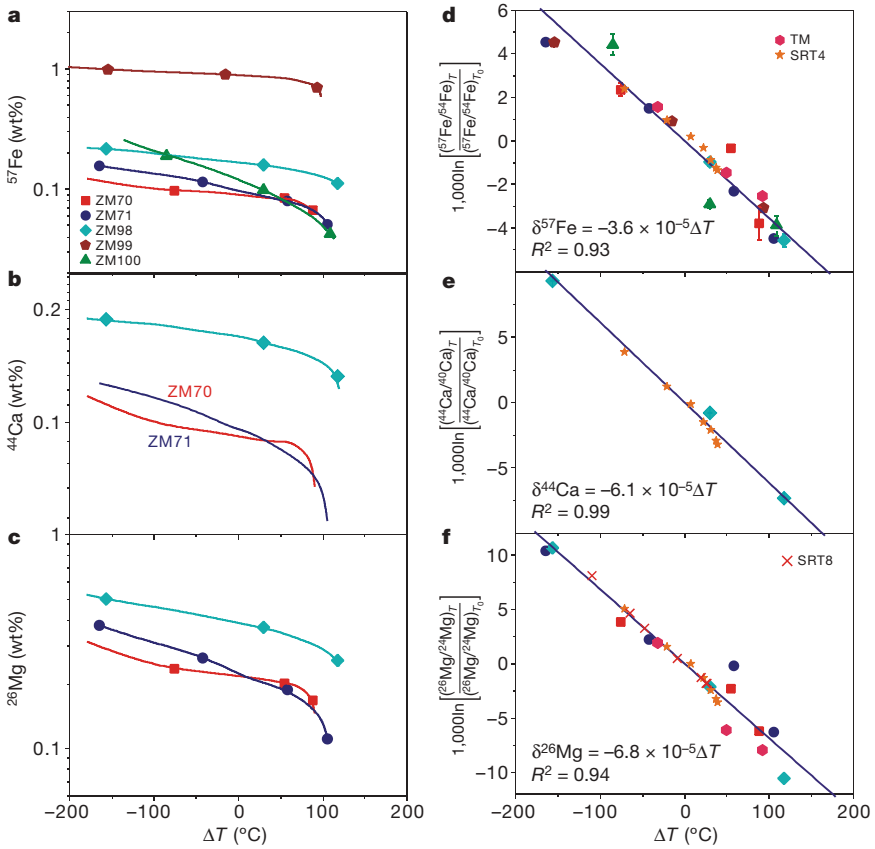

Figure 3 | Distribution of isotope concentrations and isotope ratios against ΔT for thermal diffusion experiments with a wide range of melt compositions and bulk temperatures. We choose T_0 to be the temperature of the location where the isotope ratio of the sample equals that of the starting material. **a–c**, Isotope concentrations ^{57}Fe, ^{44}Ca and ^{26}Mg (logarithmic scale) versus ΔT. The solid lines depict the concentration distribution as measured using an electron microprobe[6,16], and the symbols depict the locations where we have micro-drilled the sample to measure the isotope ratios shown in panels **d–f**. **d–f**, Logarithm of isotope ratios (^{57}Fe/^{54}Fe, ^{44}Ca/^{40}Ca and ^{26}Mg/^{24}Mg) or, equivalently, approximate isotope ratios in delta notation (1,000δ^{57}Fe, 1,000δ^{44}Ca and 1,000δ^{26}Mg) versus ΔT. From the slopes of the best-fit lines, we find that $\Delta S_T = (3.6 \times 10^{-5})\ ^\circ C^{-1}$ for ^{57}Fe/^{54}Fe, $(6.1 \times 10^{-5})\ ^\circ C^{-1}$ for ^{44}Ca/^{40}Ca and $(6.8 \times 10^{-5})\ ^\circ C^{-1}$ for ^{26}Mg/^{24}Mg. The systematic steepening of data points close to the hot end may be due to higher-order effects of temperature on ΔS_T. SRT4 and SRT8 are from refs 17, 18. Most error bars (2σ; Table 1) are smaller than the symbols. Symbols throughout are as defined in **a**, **d** and **f**.

The discovery that isotopic fractionation of iron, calcium and magnesium is independent of melt composition and temperature considerably simplifies the practical application of these isotope systems as tools for elucidating temperature-gradient processes in the evolution of the Earth. In fact, workers concerned with the origin of igneous rocks in the early 1900s seized on the newly discovered thermal diffusion phenomenon driven by the Earth's ever-present geothermal gradient as a possible mechanism for producing the compositional diversity of the continental crust. Although the idea has since lost favour to modern concepts of fractional crystallization and partial melting, there may yet be a role for thermal diffusion in the origin of some granites and the continental crust[14]. Unlike 150 years ago, however, new investigations can be guided, and the role of thermal diffusion possibly identified, by this definitive isotopic signature of thermal diffusion, which has thus far been documented only in the laboratory.

METHODS SUMMARY

We micro-drilled samples from silicate glass in thermal diffusion experiments[6,16], using tungsten carbide drill bits. The width of the drilling bands was ~0.4–0.5 mm. Temperature offsets between the drilling areas were estimated assuming first a linear and then a parabolic temperature profile across the thermal diffusion experiment. The difference in temperature estimation from the two methods is <5%.

Samples were digested in a 3:1 mixture of concentrated hydrofluoric acid and HNO_3. After iron was separated by anion resin (Bio-Rad AG1-X8), magnesium and calcium were separated from most matrix interferences using cation resin (Bio-Rad AG50-X12). Magnesium and iron procedural blanks were negligible. Yields and matrix in purified solution were checked before isotope measurement.

Iron isotopes were measured using high resolution multi-collector inductively-coupled-plasma mass spectroscopy (Nu Plasma HR, Nu Instruments) in static mode using a sample-standard bracketing method with resolutions >8,000 to resolve isobaric inferences. IRMM-014 solutions with an iron concentration equivalent to that of the samples (1.5 or 0.4 p.p.m.) were used as the bracketing standard. Magnesium isotopes were measured at a resolution of ~400 using a sample-standard bracketing method relative to an in-house magnesium standard with $\delta^{26}Mg_{DSM\text{-}3} = 3.314 \pm 0.234‰$ and $\delta^{25}Mg_{DSM\text{-}3} = 1.700 \pm 0.137‰$ (over five months; $n = 28$). Samples were diluted to approximately 0.15 p.p.m. and introduced using a DSN-100 Desolvation Nebuliser System (Nu Instruments), producing a ^{24}Mg signal of ~16 V. Calcium isotopes were measured on a thermal ionization mass spectrometer (Thermo Finnigan TRITON) in the Saskatchewan Isotope Laboratory, University of Saskatchewan, using a ^{43}Ca–^{42}Ca double spike to correct for instrumental mass fractionation.

Full Methods and any associated references are available in the online version of the paper at www.nature.com/nature.

Received 15 October 2009; accepted 13 January 2010.

1. Ludwig, C. Diffusion zwischen ungleich erwärmten Orten gleich zusammengesetzter Lösungen. *Sitz. Math. Naturwiss. Classe Kaiserlichen Akad. Wiss.* **20**, 539 (1856).
2. Soret, C. Sur l'état d'équilibre que prend au point de vue de sa concentration une dissolution saline primitivement homohéne dont deux parties sont portées à des températures différentes. *Arch. Sci. Phys. Nat.* **2**, 48–61 (1879).
3. Astumian, R. D. Coupled transport at the nanoscale: the unreasonable effectiveness of equilibrium theory. *Proc. Natl Acad. Sci. USA* **104**, 3–4 (2007).
4. Debuschewitz, C. & Köhler, W. Molecular origin of thermal diffusion in benzene + cyclohexane mixtures. *Phys. Rev. Lett.* **87**, 055901 (2001).

5. Duhr, S. & Braun, D. Thermophoretic depletion follows Boltzmann distribution. *Phys. Rev. Lett.* **96,** 168301 (2006).
6. Lesher, C. E. & Walker, D. Solution properties of silicate liquids from thermal diffusion experiments. *Geochim. Cosmochim. Acta* **50,** 1397–1411 (1986).
7. Platten, J. K. The Soret effect: a review of recent experimental results. *J. Appl. Mech.* **73,** 5–15 (2006).
8. Putnam, S. A., Cahill, D. G. & Wong, G. C. L. Temperature dependence of thermodiffusion in aqueous suspensions of charged nanoparticles. *Langmuir* **23,** 9221–9228 (2007).
9. Tyrrell, H. J. V. *Diffusion and Heat Flow in Liquids* (Butterworth, 1961).
10. Duhr, S. & Braun, D. Why molecules move along a temperature gradient. *Proc. Natl Acad. Sci. USA* **103,** 19678–19682 (2006).
11. Braun, D. & Libchaber, A. Thermal force approach to molecular evolution. *Phys. Biol.* **1,** 1–8 (2004).
12. Severinghaus, J. P., Grachev, A. & Battle, M. Thermal fractionation of air in polar firn by seasonal temperature gradients. *Geochem. Geophys. Geosyst.* **2,** 1048 (2001).
13. Severinghaus, J. P. *et al.* Timing of abrupt climate change at the end of the Younger Dryas interval from thermally fractionated gases in polar ice. *Nature* **391,** 141–146 (1999).
14. Lundstrom, C. C. Hypothesis for the origin of convergent margin granitoids and Earth's continental crust by thermal migration zone refining. *Geochim. Cosmochim. Acta* **73,** 5709–5729 (2009).
15. Groot, S. R. D. *Thermodynamics of Irreversible Processes* 111–118 (North-Holland, 1959).
16. Lesher, C. E. & Walker, D. in *Diffusion, Atomic Ordering, and Mass Transport* (ed. Ganguly, J.) 396–451 (Adv. Phys. Geochem. 8, Springer, 1991).
17. Richter, F. M. *et al.* Isotopic fractionation of the major elements of molten basalt by chemical and thermal diffusion. *Geochim. Cosmochim. Acta* **73,** 4250–4263 (2009).
18. Richter, F. M. *et al.* Magnesium isotope fractionation in silicate melts by chemical and thermal diffusion. *Geochim. Cosmochim. Acta* **72,** 206–220 (2008).
19. Wittko, G. & Kohler, W. Universal isotope effect in thermal diffusion of mixtures containing cyclohexane and cyclohexane-d12. *J. Chem. Phys.* **123,** 014506 (2005).
20. Wittko, G. & Kohler, W. On the temperature dependence of thermal diffusion of liquid mixtures. *Europhys. Lett.* **78,** 46007 (2007).
21. Furry, W. H., Jones, R. C. & Onsager, L. On the theory of isotope separation by thermal diffusion. *Phys. Rev.* **55,** 1083–1095 (1939).
22. Kyser, T. K., Lesher, C. E. & Walker, D. The effects of liquid immiscibility and thermal diffusion on oxygen isotopes in silicate liquids. *Contrib. Mineral. Petrol.* **133,** 373–381 (1998).
23. Ott, A. Isotope separation by thermal diffusion in liquid metal. *Science* **164,** 297 (1969).
24. Reith, D. & Muller-Plathe, F. On the nature of thermal diffusion in binary Lennard-Jones liquids. *J. Chem. Phys.* **112,** 2436–2453 (2000).
25. LaTourrette, T., Wasserburg, G. J. & Fahey, A. J. Self diffusion of Mg, Ca, Ba, Nd, Yb, Ti, Zr, and U in haplobasaltic melt. *Geochim. Cosmochim. Acta* **60,** 1329–1340 (1996).
26. Lesher, C. E. Kinetics of Sr and Nd exchange in silicate liquids theory, experiments, and applications to uphill diffusion, isotopic equilibration, and irreversible mixing of magmas. *J. Geophys. Res.* **99,** 9585–9604 (1994).
27. van der Laan, S., Zhang, Y., Kennedy, A. K. & Wyllie, P. J. Comparison of element and isotope diffusion of K and Ca in multicomponent silicate melts. *Earth Planet. Sci. Lett.* **123,** 155–166 (1994).
28. Lesher, C. E. Decoupling of chemical and isotopic exchange during magma mixing. *Nature* **344,** 235–237 (1990).
29. Zhang, Y. A modified effective binary diffusion model. *J. Geophys. Res.* **98,** 11901–11920 (1993).
30. Huang, F. *et al.* Chemical and isotopic fractionation of wet andesite in a temperature gradient: experiments and models suggesting a new mechanism of magma differentiation. *Geochim. Cosmochim. Acta* **73,** 729–749 (2009).

Supplementary Information is linked to the online version of the paper at www.nature.com/nature.

Acknowledgements This work is supported by US National Science Foundation grants NSF EAR 0609726 and NSF EAR 0944169 (C.C.L.), and NSF EAR 0943991 (C.E.L.). The multi-collector inductively-coupled-plasma mass spectrometry laboratory at the University of Illinois at Urbana-Champaign is supported by NSF EAR 0732481. P.C. acknowledges support from a Roscoe G. Jackson II Research Fellowship. P.C. and S.W.K. acknowledge support from S.W.K.'s Walgreen Chair funds. We thank B. Fouke for use of his micro-drilling system, Z. Zhang and X. Li for analytical assistance, V. Kariwala for help with references and Y. Zhang for a review of this work.

Author Contributions F.H. led the analytical effort and P.C. led the theoretical treatment of the results. C.E.L. performed the laboratory thermal diffusion experiments. J.J.G.G. assisted with iron and magnesium isotope analyses and C.H. measured calcium isotopes. P.C. and F.H. wrote the manuscript and Supplementary Information with contributions from C.C.L., C.H., S.W.K., J.J.G.G. and C.E.L.

Author Information Reprints and permissions information is available at www.nature.com/reprints. The authors declare no competing financial interests. Correspondence and requests for materials should be addressed to C.C.L. (lundstro@illinois.edu).

METHODS

Thermal diffusion experiments. Silicate melts of variable bulk composition were placed at above liquidus temperatures in the temperature gradient of a piston cylinder apparatus for the times given in Table 1. The chemical compositions of the starting materials ranged from mid-ocean-ridge basalt (ZM98) and andesite (ZM70 and ZM71) to rhyolitic pantellerite (ZM100) and synthetic melt Fe_2SiO_4–$KAlSiO_4$–SiO_2 (ZM99) (Table 1). We also included data from a recent thermal migration study on andesite, which involved coexisting silicate melt and minerals in a temperature gradient[30], and other thermal diffusion experiments using basalt as starting material[17,18]. In addition to the wide range in composition, the data also span a wide range in temperature: the temperature at the hot end ranged from 950 to 1,650 °C and that at the cold end ranged from 350 to 1,415 °C. Generally, in thermal diffusion experiments iron, calcium and magnesium migrate to, and become enriched at, the cold end of the experiments, whereas silicon behaves oppositely[6,16]. All experiments except ZM70 were of long enough duration to evolve to within 95% of the steady-state condition in terms of concentration changes of major elements.

Iron, magnesium and calcium isotope analyses. Samples were micro-drilled from silicate glass in thermal diffusion experiments[6,16]. To avoid contamination of iron by the micro-drilling process, we used tungsten carbide drill bits to drill 0.4–0.5-mm-wide bands across the silicate glass in the polished surface mount section of the experiments reported in refs 6, 16. These widths translate into a temperature range of ~10 °C. Temperature differences between the drilling areas were estimated assuming both a linear and a parabolic temperature profile across the thermal diffusion experiment. The difference in temperature estimated by the two methods is negligible (the values are within 5% of each other).

After micro-drilling, the silicate glass powder was digested in 7-ml Teflon beakers using a 2-ml 3:1 mixture of concentrated hydrofluoric acid and HNO_3. Iron and magnesium were separated by anion resin (Bio-Rad AG1-X8) and cation resin (Bio-Rad AG50-X12), respectively. The iron and magnesium blanks for the chemical separation process had masses of <10 ng and 3 ng, respectively. These are negligible in comparison with the amounts of iron and magnesium in the samples (>2 μg). The iron and magnesium blanks for the micro-drilling process had masses of <7 ng and 1 ng, respectively. Yields and matrix were checked before isotopic measurements to ensure excellent recovery and purification.

Iron isotopes were measured by high-resolution multi-collector inductively-coupled-plasma mass spectroscopy (Nu Plasma HR, Nu Instruments) in the Department of Geology at the University of Illinois at Urbana-Champaign, in static mode using a sample-standard bracketing method relative to IRMM-014 as the bracketing standard. Samples were diluted to 1.5 p.p.m. iron (ZM71, ZM98 and ZM99) or to 0.4 p.p.m. iron (ZM70 and ZM100). Iron solutions were introduced into the mass spectrometer with a desolvating nebulizer (DSN-100, Nu Instruments) in 2% HNO_3, producing a ^{56}Fe signal sensitivity of ~10 V per p.p.m. Interferences of ArN^+ and ArO^+ were adequately resolved with resolutions greater than 8,000. Isotope beams of ^{57}Fe, ^{56}Fe and ^{54}Fe were measured in Faraday cups with 10^{11}-Ω resistor channels. The measured $^{56}Fe/^{54}Fe$ and $^{57}Fe/^{54}Fe$ ratios were corrected for the isobaric interference of ^{54}Cr using ^{53}Cr simultaneously measured on detector L5. The long-term (six-month) average $\delta^{56}Fe_{IRMM\text{-}014}$ values from 28 analyses of ETH hematite and 55 analyses of in-house standard (UIFe) are 0.585 ± 0.049‰ and 0.708 ± 0.093‰ (2σ), respectively. The error in the $\delta^{56}Fe_{IRMM\text{-}014}$ values of the samples is up to 0.28‰ (for the solutions with 0.4 p.p.m. iron), which is insignificant relative to the isotopic variation (>5‰) of the thermal experiments.

Magnesium isotopes were measured using the Nu Plasma HR mass spectrometer at resolution of about 400, using a sample-standard bracketing method relative to an in-house magnesium standard. The $\delta^{26}Mg_{DSM\text{-}3}$ and $\delta^{25}Mg_{DSM\text{-}3}$ values of the in-house bracketing standard over five months are 3.314 ± 0.235‰ and 1.700 ± 0.137‰ (2σ, $n = 28$), respectively. Samples were diluted to approximately 0.15 p.p.m. and introduced using the DSN-100, producing a ^{24}Mg signal of ~16 V. Isotope beams of ^{26}Mg, ^{25}Mg and ^{24}Mg were measured simultaneously. Matrix and yields were checked before each run, with $^{23}Na/Mg$ and $^{27}Al/Mg$ generally less than 5%. Details of the magnesium analytical procedure are available in ref. 31.

Calcium isotopes were measured on a thermal ionization mass spectrometer (Thermo-Finnigan TRITON) in the Saskatchewan Isotope Laboratory using a ^{43}Ca–^{42}Ca double spike to correct for instrumental mass fractionation (see ref. 32). Before mass spectrometric analysis, calcium was purified from matrix elements, including potentially interfering ^{40}K, using conventional cation exchange chromatography. The data are reported in the conventional delta notation as $\delta^{44}Ca_{SW} = (^{44}Ca/^{40}Ca_{sample})/(^{44}Ca/^{40}Ca_{SW}) - 1$. The standard is natural sea water. The external precision of $\delta^{44}Ca$ values is ±0.07‰ (2σ) on the basis of repeated analyses of sea water and an internal laboratory CaF_2 standard. The average $\delta^{44}Ca$ value for NIST SRM 915a measured in the Saskatchewan Isotope Laboratory is −1.86‰.

31. Huang, F. *et al.* Magnesium isotopic composition of igneous rock standards measured by MC-ICP-MS. *Chem. Geol.* **268**, 15–23 (2009).
32. Holmden, C. & Bélanger, N. Ca isotope cycling in a forested ecosystem. *Geochim. Cosmochim. Acta* **74**, 995–1015 (2010).

SUPPLEMENTARY INFORMATION

Supplementary Information: Isotope fractionation in silicate melts by thermal diffusion

F. Huang[1⋆], P. Chakraborty[1⋆], C. C. Lundstrom[1], C. Holmden[2], J. J. G. Glessner[1], S. Kieffer[1], C.E. Lesher[3]

[1]*Department of Geology, University of Illinois, Urbana, IL 61801, USA.*

[2]*Department of Geological Sciences, University of Saskatchewan, Saskatoon SK S7N 5E2, Canada.*

[3]*Department of Geology, University of California, Davis, CA 95616, USA.*

⋆ *These authors contributed equally to this work.*

Supplementary Discussion

Relation between δ and logarithm of ratio of the isotope concentrations

Recall that in the δ notation, the concentration ratio of isotopes $^{\mathrm{X}}\mathrm{M}$ and $^{\mathrm{Y}}\mathrm{M}$ is expressed as

$$\delta^{\mathrm{X}}\mathrm{M} = \frac{(^{\mathrm{X}}\mathrm{M}/^{\mathrm{Y}}\mathrm{M})_{sample}}{(^{\mathrm{X}}\mathrm{M}/^{\mathrm{Y}}\mathrm{M})_{starting\_material}} - 1. \tag{S-1}$$

(We note that when δ is reported in the units of ‰, a multiplying factor of $1,000$ is used in the above expression; see equation 2 of the manuscript.) Considering the sample at a location with temperature T and denoting the temperature of the location where the isotope ratio of the sample

equals that of the starting material as T_0, we can rewrite the above equation as

$$1 + \delta^{\mathrm{X}}\mathrm{M} = \frac{(^{\mathrm{X}}\mathrm{M}/^{\mathrm{Y}}\mathrm{M})_T}{(^{\mathrm{X}}\mathrm{M}/^{\mathrm{Y}}\mathrm{M})_{T_0}}. \tag{S-2}$$

We note that due to mass conservation, T_0 lies between the temperatures of the hot end and the cold end. Taking the natural logarithm of the above equation, and noting that $\delta^{\mathrm{X}}\mathrm{M} \ll 1$ (thus, $\ln(1 + \delta^{\mathrm{X}}\mathrm{M}) \approx \delta^{\mathrm{X}}\mathrm{M}$), we obtain

$$\delta^{\mathrm{X}}\mathrm{M} \approx \ln \frac{(^{\mathrm{X}}\mathrm{M}/^{\mathrm{Y}}\mathrm{M})_T}{(^{\mathrm{X}}\mathrm{M}/^{\mathrm{Y}}\mathrm{M})_{T_0}}. \tag{S-3}$$

We have used equation S-3 in equation (4) of the manuscript.

Relationship between ΔS_T and linear correlation in figure 2

Here we show that a constant ΔS_T for isotopes of an element is a sufficient condition for the δ vs. δ relationship for different elements to be linear (as is seen in Fig. 2). (We note that a necessary condition[1] is a "condition which must hold for a result to be true, but which does not guarantee it to be true" and a sufficient condition[1] is a "condition which, if true, guarantees that a result is also true," but, "the result may also be true if the condition is not met.")

Consider elements A and B. Since ΔS_T is a constant for isotopes of an element, from equation 4 of the manuscript we get

$$\delta A = (\Delta S_T)_A \Delta T, \tag{S-4}$$

$$\delta B = (\Delta S_T)_B \Delta T. \tag{S-5}$$

By eliminating ΔT from the above equations, we obtain

$$\delta A = \frac{(\Delta S_T)_A}{(\Delta S_T)_B} \delta B. \tag{S-6}$$

The above equation shows that δA and δB are linearly related with a slope set by the ratio of the ΔS_T of the elements. In the following table we show the comparison between slopes of the best-fit lines to the experimental data in Fig. 2 with the slope obtained using the above equation (we get the values of ΔS_T from Fig. 3):

Fig. 2	best-fit slope	slope from equation (S-6)
(A) δ^{26}Mg vs. δ^{57}Fe	1.9	1.9
(B) δ^{44}Ca vs. δ^{57}Fe	1.5	1.7
(C) δ^{44}Ca vs. δ^{26}Mg	0.79	0.90

We find that the slope of the experimental data is in good accord with equation (S-6).

We note that for the δ vs. δ relationship for different elements to be linear, the requirement that ΔS_T for isotopes of an element be a constant is not a necessary condition. The condition that ΔS_T does not depend on the melt composition is a necessary condition, but ΔS_T can depend on the temperature. The linearity of the δ-δ relation is predicated upon the temperature dependence of ΔS_T being separable. For example, consider the following functional form of ΔS_T

$$\Delta S_T(T, p) = f(T)g(p), \tag{S-7}$$

where p denotes properties of the isotope (e.g. mass), and f and g are unknown functions of T and

p, respectively. Next we show that equation (S-7) is a sufficient condition for the linearity of δ-δ relation.

Using equation (S-7) we can write equation (4) from the manuscript as

$$\delta^{\mathrm{X}}\mathrm{M} = g(p) \int_{T_0}^{T} f(T)dT. \tag{S-8}$$

Considering elements A and B and noting that the integral in the above equation is the same for the two elements, we follow the steps outlined above and get

$$\delta A = \frac{g(p)_A}{g(p)_B}\delta B. \tag{S-9}$$

The above equation shows that δA and δB are linearly related.

Data fitting: functional form of f_m and ΔS_T

Here we obtain a functional form of f_m (refer to equation 5 of the manuscript), and thus of ΔS_T, via data fitting. We note that for isotope pair $^{\mathrm{X}}\mathrm{M}$ and $^{\mathrm{Y}}\mathrm{M}$, these two functions are related by

$$\Delta S_T(X, Y, \dots) = f_m(X, \dots) - f_m(Y, \dots). \tag{S-10}$$

We assume that the function f_m depends on mass m and field strength Z^2/a of the isotopes, and on c (a mass-independent dimensional constant whose physical significant remains unknown in this analysis). In light of the above assumptions, we postulate the following empirical power-law

$$f_m(m, Z^2/a, c) = cm^{\alpha}\left(\frac{Z^2}{a}\right)^{\beta}. \tag{S-11}$$

We want to find the exponents α and β. Using the above equation, equation (S-10) can be expressed as

$$\Delta S_T(X, Y, Z^2/a, c) = c\left(\frac{Z^2}{a}\right)^{\beta}\left(X^{\alpha} - Y^{\alpha}\right). \tag{S-12}$$

We use the results for the experiments, which are shown in the following table (where we take the ΔS values from the best-fit lines of figure 3 in the manuscript, and the a values from ref[2]):

element	ΔS_T ($^\circ$C^{-1})	a (Å)	Z	X	Y
^{57}Fe-^{54}Fe	3.6 $\times 10^{-5}$	0.78	+2	57	54
^{26}Mg-^{24}Mg	6.8 $\times 10^{-5}$	0.72	+2	26	24
^{44}Ca-^{40}Ca	6.1 $\times 10^{-5}$	1.00	+2	44	40

Using the above data, we solve equation (S-11) to obtain $\alpha \approx -1/4$ and $\beta \approx 9/20$. Thus we have the following functional form

$$f_m \propto m^{-1/4}\left(\frac{Z^2}{a}\right)^{9/20}. \tag{S-13}$$

We note that the above functional form is predicated on fitting the above data for Fe, Mg, and Ca. By combining equations (S-13) and (S-12), we can write

$$\Delta S_T = c\left(\frac{Z^2}{a}\right)^{9/20}\left(X^{-1/4} - Y^{-1/4}\right). \tag{S-14}$$

Last, we discuss the parameters that appear in the argument of S_T, or equivalently, as per equation (5), the parameters that appear in the arguments of functions f_m and f_c. As noted in the manuscript, in considering isotope ratios, the effects of f_c cancel out, leaving only the effects of f_m.

Thus, isotope ratio data can only provide information on the parameters of the argument of f_m, and therefore, of ΔS_T. In the discussion above we assumed that f_m depends on mass, field strength, and an unknown mass-independent dimensional constant. Fitting the available data resulted in equation (S-14). Further experiments on more isotope systematics (from light and small, H and Li, to heavy and big, U) are needed to better identify the parameters (such as, cation volume) that affect ΔS_T.

Supplementary Table

Table S1 Concentration (in weight %) of ^{26}Mg, ^{44}Ca, and ^{57}Fe in silicate melts (Fig. 3a-c). We computed the concentrations based on micro-drilling position and melt data in references 6 and 16.

sample	^{26}Mg	^{44}Ca	^{57}Fe
ZM70A	0.17		0.067
ZM70B	0.20		0.084
ZM70C	0.24		0.097
ZM71A	0.11		0.051
ZM71B	0.19		0.080
ZM71C	0.27		0.115
ZM71D	0.38		0.157
ZM98A	0.26	0.13	0.112
ZM98B	0.37	0.16	0.160
ZM98C	0.50	0.19	0.216
ZM99A			0.700
ZM99B			0.901
ZM99C			0.990
ZM100A			0.042
ZM100B			0.098
ZM100C			0.189

Supplementary Notes

1. Weisstein, E. W. Mathworld—a wolfram web resource (http://mathworld.wolfram.com).

2. Shannon, R. D. Revised effective ionic radii and systematic studies of interatomic distances in halides and chalcogenides. *Acta Crystallographica Section A* **32**, 751–767 (1976).